

## Modeling the Multicomponent Compositional Effects of Asphaltenes on Interfacial Phenomena

Fang Liu,\* Vincent Pauchard, and Sanjoy Banerjee



Cite This: *Energy Fuels* 2020, 34, 13673–13685



Read Online

ACCESS |

Metrics & More

Article Recommendations

Supporting Information

**ABSTRACT:** The polydisperse nature of asphaltenes is not usually considered in studies of asphaltenes adsorption effects at interfaces, e.g., water–oil interfaces. We recently proposed a methodology that takes into account the mixture nature of asphaltenes and showed that a binary mixture model for diffusion-limited adsorption at water–oil interfaces could describe qualitatively all of the features of asphaltenes’ interfacial dilatational rheology [Liu, F.; et al. *Langmuir* 2017, 33, 1927–1042, DOI: 10.1021/acs.langmuir.6b03958]. On the quantitative side, however, use of only two pseudocomponents did not adequately predict some other aspects of their behavior, such as dynamic interfacial tension over the full range of time scales. To address these limitations, a methodology for calculating interfacial rheological properties for an *n*-component mixture was first developed [Liu, F.; et al. *Colloids Surf. A* 2017, 532, 140–143, DOI: 10.1016/j.colsurfa.2017.05.080]. To capture, first, the interfacial tension behavior and then the rheological properties within the same methodological structure, we discuss here an approach using a multicomponent model that inversely solves the Ward–Tordai equations and extracts the properties of individual pseudocomponents (concentration and adsorption coefficient) from dynamic interfacial tension measurements. Using ternary mixture models proves sufficient to capture the data obtained for asphaltenes over large adsorption time scales (up to 24 h) and large frequency range. Quaternary mixture models do not significantly improve the predictions. Another feature revealed by this methodology is the aggregation behavior of the different pseudocomponents. For dilute solutions, the calculated sum of the pseudocomponents’ concentrations falls in the range of the actual asphaltenes concentration. As the actual asphaltenes concentration is increased, the calculated concentration of the most surface-active pseudocomponents levels off, indicating that the most surface-active asphaltenes are also the most prone to aggregate due perhaps to  $\pi$ – $\pi$  interactions. This result would be expected as asphaltenes adsorption at the water–oil interface appear to be driven by the interactions of the  $\pi$  electrons of their aromatic cores as previously demonstrated [Rane, J. P.; et al. *Energy Fuels* 2015, 29, 3584–3590, DOI: 10.1021/acs.energyfuels.5b00179]. Finally, the result obtained by this model indicates that the presence of a very small fraction of extremely surface-active asphaltenes components could explain both the “everlasting” interfacial tension decay observed and the apparent irreversibility of adsorption during washout experiments.

### 1. INTRODUCTION

Asphaltenes, as one of the most surface-active components in crude oil, play an important role in the stabilization of the water-in-oil emulsion. Although asphaltenes adsorption at fluid–fluid interfaces has been extensively studied,<sup>1–13</sup> their adsorption mechanisms still remain in debate. It was often observed that the phenomenon associated with the adsorption process is quite slow, even at high asphaltenes concentration.<sup>2,14,15</sup> The equilibration time was found to be much longer than the characteristic time scale of the diffusion-controlled adsorption process, as calculated with a single-component hypothesis.<sup>14</sup> On the basis of a fit of interfacial tension (IFT) data with a model developed for protein adsorption, Jeribi et al.<sup>14</sup> concluded that asphaltenes endured an initial rapid diffusion and later a long interfacial reorganization on the surface plane. This argument was supported by many studies on dilatational rheology. For example, it was observed that a composite model combining diffusion-controlled adsorption of a single surfactant (the Lucassen van den Tempel (LVDT) model) and some intrinsic viscoelastic properties were needed to match the dilatational rheology of asphaltenes-laden interfaces.<sup>16</sup> Similarly, the

observed power-law dependence of dilatational moduli over frequency (the so-called critical gel rheology) seemingly confirmed the formation of some kind of gelled interface preventing water droplet coalescence.<sup>17–20</sup> However, the slow formation of an interfacial asphaltenes network due to molecular reorientation contradicted with the observation that water-in-oil emulsion can be stabilized over a few minutes when mixed with asphaltenes.<sup>6,8,21–24</sup> Clearly the experimental evidence on rapid emulsion stabilization by asphaltenes in stirred (turbulent) oil–water systems did not agree with the slow formation of networked asphaltenes at interfaces that impeded coalescence.

Recently, a series of articles offered a different perspective on the subject.<sup>1,4,6,7,25–28</sup> Focusing on experimental conditions that prelude dynamic exchange, they demonstrated that in the

Received: July 19, 2020

Revised: October 10, 2020

Published: November 3, 2020



presence of asphaltenes, surface pressure, and limiting elasticity follow an equation of state and they depend on surface coverage only. By means of viscosity variation and asymptotic analysis, it was also demonstrated that dynamic interfacial tensions were largely governed by mass transport (i.e., diffusion in quiescent media, such as in a pendant droplet apparatus, or advection in a stirred emulsion, introducing the effect of time scales for different processes, e.g., into emulsion stability and dynamic interfacial tension). Furthermore, it was observed in the literature that the experimental dependency of dilatational moduli over asphaltenes concentration always exhibits the first order features of diffusional relaxation (either for a single surfactant or for a mixture): elastic and viscous moduli both exhibit a maximum at intermediate concentration (following a bell-shaped curve), and elastic modulus is always higher than viscous modulus (i.e., phase angle is always less than 45°; see ref 29 and reference therein).

Consequently, the question arose: whether or not the above-mentioned deviation of asphaltene dynamic adsorption behavior from single-component diffusion-limited models could be explained by mixture effects. Essentially, asphaltenes are by definition a solubility class mainly composed of polycyclic aromatic hydrocarbons. Their detailed composition depends on their origin and the precipitating solvent,<sup>30–33</sup> but they always exhibit a great variety in molecular structure (aromaticity, molecular weights, lengths of alkyl chains, and the presence of heteroatoms).<sup>4,31,34,35</sup> Such a variety in structure would be expected to cause a great variety in adsorption properties and particularly in adsorption coefficient. This point has however received little attention so far. In a seminal work, Fossen et al.<sup>30</sup> have shown that fractionating asphaltenes using different precipitants yielded very different dynamic interfacial tension curves. On the other hand, many experimental studies<sup>33,36–43</sup> have attempted to isolate asphaltene subfractions responsible for water–oil emulsion stability (either by prefractionation or by isolation of interfacial material). All results are consistent: only a small subfraction of asphaltenes adsorbs significantly at the water–oil interface and is responsible for emulsion stability.

On the basis of all of these observations, a dilatational rheology model with diffusion-controlled relaxation of two surfactants differing only in adsorption coefficients has recently been tested both qualitatively and quantitatively against dilatational rheology measurements in the presence of asphaltenes.<sup>29</sup> It has first proved to reproduce qualitatively the concentration, time, and frequency dependencies of moduli, including the so-called critical gel rheology. On a quantitative perspective, the frequency dependence of dilatational moduli as measured for a toluene/water interface after 16 h aging has been used to extract the properties (subsurface concentration and adsorption coefficient) of two pseudocomponents. These were meant to represent the asphaltenes subfraction dominating the long-term interfacial behavior, i.e., the surface-active fraction. Then, the Ward–Tordai equation (for diffusion-controlled adsorption toward an initially clean interface) has been used to adjust the pseudocomponents' bulk concentrations so that the calculated subsurface concentrations after 16 h match with the values that are initially deducted from rheology experiments. The sum of the two bulk concentrations is less than 10% of the total asphaltenes' concentration, which is consistent with previous estimates.<sup>41,43</sup> Furthermore, with those two bulk concentrations, the Ward–Tordai equation has enabled good prediction of the

independently measured evolution of dynamic interfacial tension over 16 h, except at very short times.

This short-time discrepancy is however not unexpected for a binary mixture model calibrated with long-term rheology data. Given the complexity of the asphaltenes solubility class, even the most surface-active subfraction is bound to exhibit a mixture behavior, hence the necessity to have two pseudocomponents to capture the long-term rheology. In turn, those two pseudocomponents cannot well represent the whole range of the dynamic interfacial tension. In particular, poorly surface-active bulk asphaltenes dominate the short-term dynamic interfacial tension, due to their rapid adsorption in a diffusion-controlled process based on their high bulk concentration, which necessitates introduction of a third pseudocomponent. This component would be expected to have a high bulk concentration but relatively low surface activity.

There are several obstacles to such a strategy combining the analysis of both short-term and long-term rheological and interfacial tension properties. First, there exists no analytical model of dilatational moduli for diffusional relaxation of more than two surfactants in planar geometries (and more than one for nonplanar geometries). This difficulty can be alleviated by numerical means, with a matrix inversion method enabling calculations for any number of surfactants in a simple geometry (planar, spherical, and cylindrical).<sup>44</sup> Second, there are very few experimental studies in the literature on the frequency dependence of dilatational moduli after both short and long aging times in the presence of asphaltenes.

On the other hand, there are many experimental studies providing fairly long-term dynamic interfacial tension measurements. Such data contain the dynamics of adsorption of all of the asphaltenes fractions in an integral fashion, provided the measurements were started at a sufficiently short time scale and the experimental time was long enough.

Extracting information from such experiments on interfacial tension behavior in diffusion-controlled experiments in terms of pseudocomponent properties, however, requires solution of the inverse Ward–Tordai problem, which has never been done before. In this work, we will present a novel numerical scheme for parametric optimization against dynamic IFT data. It will be first tested against some reference cases and then applied to asphaltenes data to characterize the component compositional and surface activity features.

## 2. THEORETICAL FRAMEWORK

### 2.1. Mathematical Modeling of the Problem.

Consider one-dimensional dynamic adsorption of non-ionic surface-active agent mixture from a semi-infinite medium onto a planar interface. The surfactants are uniformly distributed in the bulk initially. The adsorption process is usually considered as controlled by the following process: (i) diffusion from the bulk phase to the subsurface; (ii) adsorption from the subsurface to the interface. The asymptotic analysis of the mixed controlled kinetics under critical micelle concentration shows that the long-time adsorption approximates the diffusion-controlled process.<sup>45</sup> To describe the diffusion of the surfactants in the bulk phase, Fick's law is applied:

$$\frac{\partial C}{\partial t} = D \frac{\partial^2 C}{\partial x^2} \quad t > 0, x > 0 \quad (1)$$

The initial conditions and the boundary conditions in the bulk phase are

$$\begin{aligned} C(x, 0) &= C_b \\ \lim_{x \rightarrow \infty} C(x, t) &= C_b \quad t > 0 \\ C(0, t) &= C_s(t) \\ \frac{\partial \Gamma(t)}{\partial x} \bigg|_{x=0} &= D \frac{\partial C_s(t)}{\partial x} \bigg|_{x=0} \\ \Gamma(0) &= 0 \end{aligned}$$

where  $\Gamma$  is the surface coverage of the surfactant in the adsorption layer,  $D$  is diffusion coefficient,  $C_b$  is the initial bulk concentration, and  $C_s$  is the concentration in the subsurface layer. Using Laplace transform, Ward and Tordai<sup>46</sup> derived the integral solution of the diffusion process:

$$\Gamma(t) = 2\sqrt{\frac{D}{\pi}} \left( C_b \sqrt{t} - \int_0^{\sqrt{t}} C_s(\tau) d\sqrt{t-\tau} \right) \quad (2)$$

This diffusion equation is applicable to each individual component in the surfactant mixture for the evolution of its surface coverage.

**2.2. Numerical Methods to Solve Ward–Tordai Equations for a Surfactant Mixture.** Assuming local equilibrium between the subsurface and surface layers, dynamic surface coverage and subsurface concentration of the  $i$ th component (i.e.,  $\Gamma_i$  and  $C_{si}$ ) in the mixture can be obtained by solving the Ward–Tordai equation combined with a selected adsorption isotherm. In the limiting case with Henry adsorption isotherm,<sup>47</sup> i.e., when surface coverage is linearly dependent on subsurface concentration, the surface pressure becomes

$$\Pi = k_B T \Gamma^\infty k C_s(t) \quad (3)$$

where  $k_B$  is the Boltzmann constant,  $T$  is temperature,  $\Gamma^\infty$  is the surface excess coverage, and  $k$  is the adsorption coefficient of the species. The analytical solution for the diffusion-controlled adsorption model with a linear isotherm has then been derived as<sup>48</sup>

$$\Pi = \Delta \gamma_{eq} \left[ 1 - \exp\left(\frac{t}{\tau_D}\right) \operatorname{erfc}\left(\sqrt{\frac{t}{\tau_D}}\right) \right] \quad (4)$$

where  $\Delta \gamma_{eq} = k_B T K_H C_b$  and the characteristic diffusion time is  $\tau_D = \frac{K_H^2}{D}$ . The term  $K_H$  is Henry's law constant.

The linear isotherm, however, holds only when inhomogeneity is absent on the surface, which is not the case for an asphaltene mixture. The Langmuir isotherm model is one among those proposed to describe adsorption of asphaltene molecules at the oil–water interface. For a mixture of surfactants, the surface excess coverage,  $\Gamma^\infty$ , is assumed to be the same for all of the components and the fractional surface coverage is defined as

$$\theta_i = \frac{k_i C_{si}}{1 + \sum k_j C_{sj}} \quad (5)$$

where  $k_i$  is the adsorption coefficient of component  $i$  and  $C_{si}$  is the individual subsurface concentration of  $i$ . As can be observed from the equation, the relation between surface

coverage and concentration is nonlinear and hence its combination with the Ward–Tordai equation requires to be solved numerically.

The numerical methods to solve the Ward–Tordai equation were explicitly described in the literature.<sup>49–51</sup>  $C_{si}$  is assumed to be linear in each small time interval  $(t_{n-j} - t_{n-j-1})$ . Unlike the previous numerical methods,<sup>49–51</sup> the time step adopted in the current model has been modified to be quadratic instead of being uniform. This modification, which is balanced by some reduction in accuracy, however, improved the computation speed and simplified the computation steps. Moreover, using a quadratic time step, the fast evolution of interfacial tension in the early stages of experiments can be captured at a comparably accurate status to that in the long term while the total computation time is still kept within a reasonable range. In each time step, the trapezoidal rule is adopted since our system is a smooth and continuous curve without singularity and outliers. Unlike other integration methods involving several simultaneous quadrature points, the trapezoidal rule only takes two points in each step and is able to improve numerical integration performance compared with higher order numerical methods. Hence, the convolution of integral  $C_{si}$  can be computed using the trapezoidal rule:

$$\begin{aligned} & \int_0^{\sqrt{t_n}} C_{si}(t_n - \tau) d\sqrt{\tau} \\ &= \frac{\sqrt{t_n - t_{n-1}}}{3} [2C_{si}(t_n) + C_{si}(t_{n-1})] \\ &+ \sum_{j=0}^{n-1} \left[ \frac{\alpha(t_n - t_{n-j-1}) - \frac{\beta}{3}}{t_{n-j} - t_{n-j-1}} C_{si}(t_{n-j}) \right. \\ & \left. + \frac{\alpha(t_{n-j} - t_n) + \frac{\beta}{3}}{t_{n-j} - t_{n-j-1}} C_{si}(t_{n-j-1}) \right] \end{aligned} \quad (6)$$

where

$$\alpha = (t_n - t_{n-j-1})^{1/2} - (t_n - t_{n-j})^{1/2}$$

$$\beta = (t_n - t_{n-j-1})^{3/2} - (t_n - t_{n-j})^{3/2}$$

With a given initial concentration and diffusion coefficient, the dynamic surface coverage of each component can be computed for any time.

**2.3. Validation of Numerical Methods for Solving Single and Binary Mixtures Model.** The developed algorithms were implemented in Python, and the numerical method was first validated with the analytical solution in the Henry isotherm case for a single component. The root mean squared deviation (RMSD) was found to be less than  $10^{-3}$  for a time frame of  $10^5$  s, which is trivial.

To investigate the effect of time step discretization, the numerical results obtained using quadratic time step were then compared with that using uniform time step for a single-component system. As a result, it gives a higher order of RMSD value for the same time frame but a dramatic decrease in computation time as predicted.

The numerical solutions for a binary mixture were also checked against the experimental data (Table 1) and simulation results of Van den Bogaert and Joos<sup>52</sup> as shown in Figure 1. In their work, Van den Bogaert and Joos<sup>52</sup> presented use of the Nelder–Mead method to solve the

Table 1. Material Parameters Used in the Experiments<sup>52</sup>

	$C$ (mol/m <sup>3</sup> )	$a^a$ (mol/m <sup>3</sup> )	$D$ (m <sup>2</sup> /s)
sodium myristate	0.1	0.029	$2.8 \times 10^{-10}$
sodium laurate	0.5	0.297	$2.8 \times 10^{-10}$

<sup>a</sup>  $a$  is the Langmuir von Szyskowski constant.

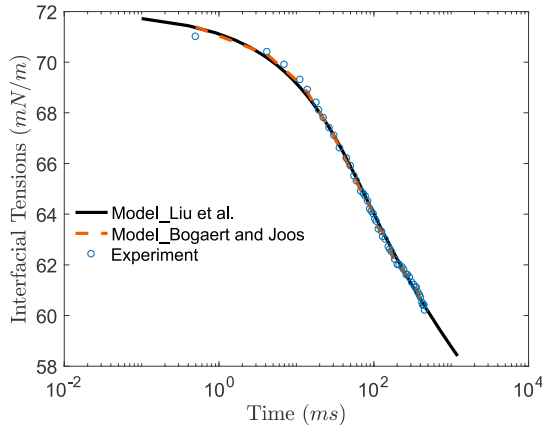


Figure 1. Numerical IFT curve generated using binary mixture model (in black). Experimental data (in blue) and numerical results (in vermilion) from Van den Bogaert and Joos.<sup>52</sup>

Ward–Todai equation for a binary mixture at each time step. This method is gradient-free and works well in high dimension but collapses on an ill-conditioned problem (i.e., very anisotropic functions).

The numerical method to solve the Ward–Tordai equation for a binary mixture model proved accurate and efficient to replicate the reference data using the same initial parameters. The RMSD value between the current numerical method and the experiment data was found to be less than  $10^{-3}$ .

**2.4. Numerical Solutions of Dilatational Rheology with Diffusional Exchange Equations for a Multi-component Mixture.** Assuming that the relaxation during oscillation is purely diffusion-controlled, the dilatational moduli of the interfaces of any geometry can be obtained by inversion matrix method, which was described in the previous publication.<sup>44</sup> The governing equation, which coupled diffusion and mass conservation, reads as follows:

$$i \Delta \Gamma_j + i \Gamma_j \frac{\Delta A}{A} + \sqrt{i \frac{D_j}{\omega}} \Delta C_{sj} = 0 \quad (7)$$

where  $\Gamma_j$  is the surface coverage of the  $j$ th component,  $A$  is the interfacial area,  $D_j$  is the diffusion coefficient,  $\omega$  is the angular frequency of the oscillations, and  $\Delta C_{sj}$  is the variation in the subsurface concentration. The variation in surface coverage and the change in subsurface concentration can be related through the adsorption isotherm:

$$\Delta \Gamma_j = \sum_1^n \frac{\partial \Gamma_j}{\partial C_{sk}} \Delta C_{sk} \quad (8)$$

Hence, there will be two linear equations and two unknowns ( $\Delta \Gamma_j$  and  $\Delta C_{sj}$ ) for each component  $j$ . The set of equations can easily be solved by separating the real part from the complex part and writing the equation sets in a matrix form. This method works for a mixture of any component at the surface of any geometry given the pure diffusion relaxation mechanism and has been validated against the analytical solution for a

single component<sup>53</sup> and the solution for binary mixture<sup>54</sup> in our previous work.<sup>44</sup>

## 2.5. Optimization Method for Model Data Fitting.

With the experimental data of dynamic interfacial tensions, to obtain the set of multiple variables  $x = \{x_1, x_2, \dots, x_n\}$  in the mixture model, i.e., the initial bulk concentrations and the adsorption coefficients of each fraction, a numerical approach is needed given the nonlinearity of the adsorption isotherm and the complexity of the Ward–Tordai equation. The problem can be formulated as a constrained nonlinear minimization problem.<sup>55</sup> The goal is to estimate the optimal set of variables,  $x$ , from minimizing the objective function,  $f(x)$ , i.e., the difference between the known experimental data set and the unknown data which will be numerically computed from the set of variables. In our case, it reads

$$\min_x f(x) = \min_x \frac{\sum_{i=1}^n (\gamma_i^{\text{num}}(x) - \gamma_i^{\text{exp}}(x))^2 w_i}{\sum_{i=1}^n w_i} \quad (9)$$

where  $\gamma$  is the interfacial tension and  $w_i$  is the weighting factor.

To solve the constrained minimization problem, an initial guess of  $x_0$  is required to start the following computation and then the selected interior-point algorithm will search possible solutions first by a direct step. If the local convex is not found at the current point, a quasi-Newton approximation, i.e., the limited-memory Broyden–Fletcher–Goldfarb–Shanno (L-BFGS) algorithm,<sup>56–60</sup> is applied to estimate the Hessian of the Lagrangian of  $f_e$  using the following equation:

$$H_k = H_{k-1} + \frac{yy^T}{y^T s} - \frac{H_{k-1} s s^T H_{k-1}}{s^T H_{k-1} s} \quad (10)$$

where

$$s = x^k - x^{k-1}$$

$$y = \nabla f(x^k) - \nabla f(x^{k-1})$$

The next step is to compute the jump direction using the Hessian matrix from the L-BFGS update,

$$\Delta x = -H_{k-1}^{-1} \nabla f(x^{k-1}) \quad (11)$$

and the new variable to be attempted becomes

$$x^k = x^{k-1} + t \Delta x \quad (12)$$

where  $t$  is the time step size. When the objective function is less than a preset limit, e.g., 0.01%, the optimization process is stopped and returns the optimal set of  $x$  variables.

Compared to the Newton method, the limited-memory BFGS update of the inverted Hessian is less costly and more stable, especially when the optimization problem goes to high dimensions and computation becomes expensive. It is also the preferred optimization method when the gradient of the objective function is unknown.

For the  $n$ -component mixture model, the current optimization problem is an  $n$ -dimension and nonconvex problem, which means multiple local minima exist for the applicable variable domain. In order to get the global minimum, a multidimensional grid of starting points was constructed in a wide distribution range and each point was randomly generated within the given range as an initial guess for each optimization process. The weighted RMSDs are then compared to select the optimal solution that gives the minimum value.

**2.6. Validation of Optimization Method.** To validate the developed optimization method, the experimental data of interfacial tensions for a binary surfactant mixture from Van den Bogaert and Joos<sup>52</sup> were used as the reference data. Using the binary mixture model based on Langmuir adsorption isotherm and the Ward–Tordai equation, the optimized parameters are listed in Table 2.

**Table 2. Optimized Parameters for a Binary Surfactant Mixture**

	C (mol/m <sup>3</sup> )	a (mol/m <sup>3</sup> )
sodium myristate	0.069	0.00046
sodium laurate	0.562	0.30800

Compared to the original values used in the reference data (see Table 1), our optimization method proved of high accuracy in the prediction of the binary mixture's composition and surface activity. The numerically generated surface tensions curve fits well with the experimental data points from Van den Bogaert and Joos<sup>52</sup> as shown in Figure 2. The

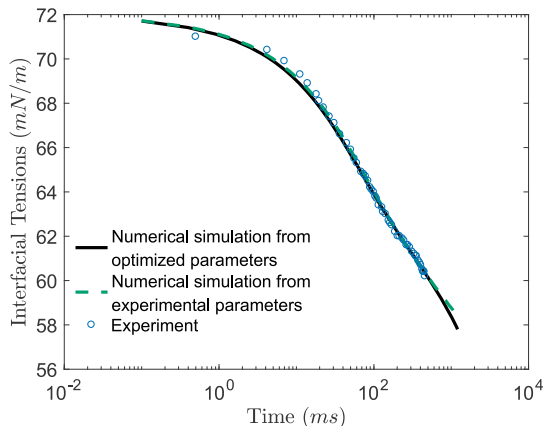


**Figure 2.** Numerical IFT curve generated from experimental (in green) and optimized (in black) parameters for a binary mixture. Experimental data (in blue) from Van den Bogaert and Joos<sup>52</sup>

activity coefficient of the minor group seems to be underestimated in the optimization probably because there were not sufficient data points available in the long time when the more surface-active component dominated the adsorption process.

In the case of ternary mixture model, few experimental/numerical data are available. The optimization method was then verified with a reference numerical data set generated using the diffusion-controlled ternary mixture model. With a random and reasonable set of six variables (i.e., concentrations and adsorption coefficients of three components), the evolution of the dynamic interfacial tensions for a three-component mixture was computed by the previously described numerical method that solves the Ward–Tordai equations. The data set was then analyzed with the algorithm for optimization to extract the initial input parameters and to verify the efficiency and accuracy of the optimization method.

The optimized result is shown against the self-generated reference data in Figure 3, and the original values with the optimized set of values are listed in Table 3.

Again, the optimized solution proved close to the real composition of the ternary mixture and the optimization

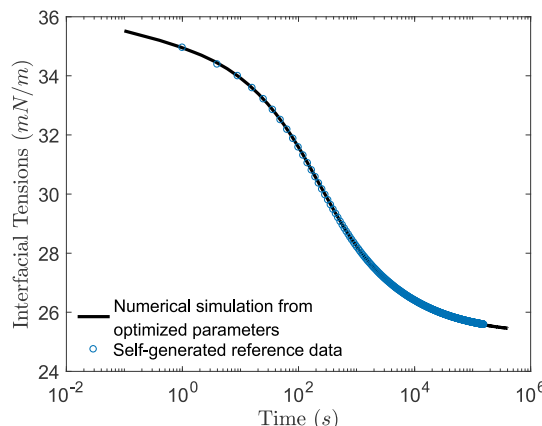


**Figure 3.** Numerical IFT curve generated from optimization for a ternary mixture model (in black). Reference data set from numerical computations of the diffusion-controlled ternary mixture model (in blue).

method was shown to be able to generate and predict the composition and surface properties of the original mixture.

### 3. RESULTS AND DISCUSSION

After the validation of both numerical computation methods and optimization methods, the next step is to apply the diffusion-controlled mixture model to analyze the adsorption kinetics of asphaltenes from experiments. Two experiment data sets were used for analysis here. One is from Yarranton's group<sup>11,61</sup> and the asphaltene samples were precipitated and prepared from Athabasca bitumen. The detailed SARA fractions were discussed in their work,<sup>62</sup> and the heptane-extracted asphaltenes take 13.8% by mass. The other one is from Radke's group,<sup>16</sup> and the asphaltenes were prepared from crude oil. The physical properties of the crude oil composition could be found in the previous study,<sup>63</sup> and the *n*-heptane insoluble asphaltenes account for 3.9 wt % in the crude oil.

There are some aspects that are specific to asphaltenes and need attention. Previous studies on dilatational rheology of asphaltenes-laden surfaces<sup>6</sup> revealed that the diffusion in the surface layer follows the Langmuir equation of state for low surface coverage. The surface excess coverage was then extracted using the Langmuir equation of state and found to be approximately 3.3 molecules/nm<sup>2</sup>, which corresponds to 6–7 polycyclic aromatic cores lying flat on the interface.<sup>4,6,34,64</sup> The diffusion coefficient was taken as an average value from literature;<sup>1,65–67</sup> i.e.,  $D = 2.5 \times 10^{-10}$  m<sup>2</sup>/s. The sensitivity analysis has been performed around the chosen values of surface excess coverage and bulk diffusion coefficient and can be found in the Supporting Information.

**3.1. Simulation of Asphaltenes Adsorption Behaviors with a Multicomponent Mixture Model.** Our previous work<sup>29</sup> has shown that a binary diffusional mixture model was able to capture the main characteristics of both interfacial tensions and dilatational rheology. However, the deviation between dynamic surface tension data and binary mixture model in the short-time range and the presence of multiple dissimilarities throughout the whole time period indicated the limitation of grouping the polydispersity of asphaltenes into two pseudocomponents. Adding more pseudocomponents into data analysis might mitigate these discrepancies between experimental data and diffusional mixture model. Hence, the same dynamic interfacial tensions data of asphaltenes'

Table 3. Original and Optimized Variables from the Three-Component Mixture Model

	$C_{b1}$ (mol/m <sup>3</sup> )	$C_{b2}$ (mol/m <sup>3</sup> )	$C_{b3}$ (mol/m <sup>3</sup> )	$k_1^a$ (m <sup>3</sup> /mol)	$k_2$ (m <sup>3</sup> /mol)	$k_3$ (m <sup>3</sup> /mol)
reference	0.00032	0.0093	0.0387	630.90	102.94	1.75
optimization	0.00028	0.0092	0.0357	691.42	105.17	1.96

<sup>a</sup> $k$  is the adsorption coefficient and is the ratio of adsorption rate constant over desorption rate constant.

Table 4. Optimized Variables from the  $n$ -Component Mixture Model (Yarranton's Data;  $C_{\text{nominal}} = 0.6661\text{ mol/m}^3$ )

	$C_{b1}$ (mol/m <sup>3</sup> )	$C_{b2}$ (mol/m <sup>3</sup> )	$C_{b3}$ (mol/m <sup>3</sup> )	$C_{b4}$ (mol/m <sup>3</sup> )	$k_1$ (m <sup>3</sup> /mol)	$k_2$ (m <sup>3</sup> /mol)	$k_3$ (m <sup>3</sup> /mol)	$k_4$ (m <sup>3</sup> /mol)
single	0.0319					51.17		
binary	0.0028	0.0666				364.21	12.22	
ternary	0.0002	0.0069	0.0904		148694.00	125.22	6.50	
quaternary	0.0002	$1.66 \times 10^{-8}$	0.0058	0.0767	5478183.77	124334.35	141.76	8.42

adsorption at water–toluene interfaces<sup>9</sup> were analyzed using the diffusion-controlled model for ternary- and quaternary-component systems.

In the ternary system, the initial total bulk concentration of the surfactant mixture was given but not the concentrations and the adsorption coefficients of the individual components, which become six to-be-optimized variables (eight variables in the quaternary case). The optimized variables of the  $n$ -component mixture were summarized in Table 4, and the corresponding IFT curves of the  $n$ -component mixture model are shown together with experimental data in Figure 4.

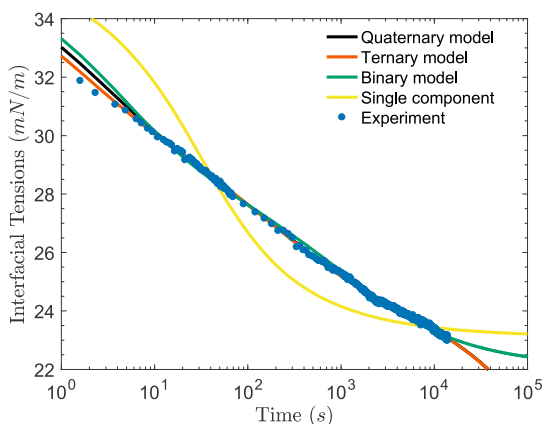


Figure 4. Numerical IFT curve generated using multicomponent mixture model (yellow, single component; green, binary mixture; vermilion, ternary system). Experimental data from Sztukowski and Yarranton<sup>11</sup> (in blue): 0.5 kg/m<sup>3</sup> asphaltenes in toluene.

In order to justify the universal applicability of the mixture model, another set of experimental data with a wide distribution in measured adsorption time and oscillation frequencies from Freer and Radke<sup>16</sup> was then analyzed using the single-, binary-, ternary-, and quaternary-system mixture model (shown in Figure 5). The optimized variables of the  $n$ -component mixture can be found in Table 5.

Compared to the single-component and binary mixture model, the ternary and quaternary mixture models fit better with the experimental data of dynamic interfacial tensions over long time periods. It is important to note that the quaternary mixture model showed no significant improvement in fitting compared with the ternary case, indicating that a ternary mixture model can sufficiently grasp the complexity of an asphaltene mixture.

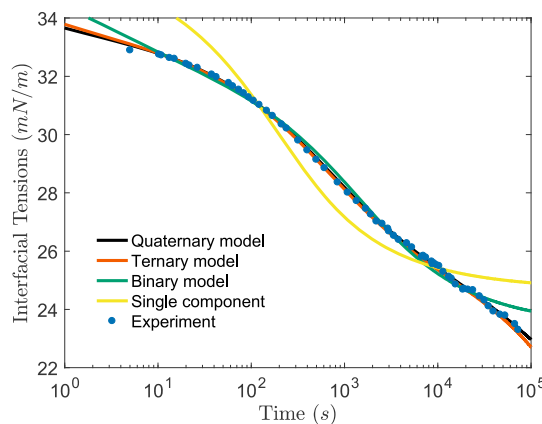


Figure 5. Numerical IFT curve generated using multicomponent mixture model (yellow, single component; green, binary mixture; vermilion, ternary mixture; black, quaternary mixture). Experimental data from Freer and Radke<sup>16</sup> (in blue dots): 0.005 wt % asphaltenes in toluene.

From the optimized initial concentrations generated by the ternary mixture model for both data sets, each pseudocomponent was found to account for a similar percentage in the mixture. Less than 10% of asphaltenes are much more surface-active than the bulk of the asphaltenes group, which was consistent with observations from other measurements.<sup>11,68</sup> The smallest fraction (<0.5%) seems to be responsible for the “everlasting” interfacial tension decay. The extreme behaviors of this minority fraction were underrepresented and not fully revealed in the single/binary system. This can be clearly observed from the evolution of individual fractional coverage in the ternary system (see Figure 6) as an example.

The fractional surface coverage of each surfactant can be calculated from the individual subsurface concentrations using eq 5. The adsorption of the most abundant but less surface-active components (pseudocomponent 3) quickly reached the maximum coverage within several decades of seconds, indicating that it is the main contributor to the initial fast decrease of IFTs. In contrast, the tiny fraction with the highest surface-activity (pseudocomponent 1) exhibited a slow and prolonged adsorption process. After reaching the maximum surface coverage within a few seconds, the less surface-active components that had adsorbed onto the water–oil interface started to gradually be replaced by the more surface-active but less numerous components. The most surface-active component seemed not to reach the maximum surface coverage within the simulated time of around 27 h.

Table 5. Optimized Variables from the *n*-Component Mixture Model (Freer and Radke's Data;  $C_{\text{nominal}} = 0.0578 \text{ mol/m}^3$ )

	$C_{b1}$ (mol/m <sup>3</sup> )	$C_{b2}$ (mol/m <sup>3</sup> )	$C_{b3}$ (mol/m <sup>3</sup> )	$C_{b4}$ (mol/m <sup>3</sup> )	$k_1$ (m <sup>3</sup> /mol)	$k_2$ (m <sup>3</sup> /mol)	$k_3$ (m <sup>3</sup> /mol)	$k_4$ (m <sup>3</sup> /mol)	RMSD(IFT)	RMSD(Rheo)
single	0.0119				111.97				12.9540	2.4272
binary	0.0036	0.0453			348.56	6.86			4.5790	1.9331
ternary	0.0002	0.0053	0.1092		58146.54	192.86	2.06		1.6119	1.3350
ternary (convex)	0.0001	0.0050	0.1070		11187.80	192.59	2.06		2.8658	1.1659
quaternary	0.00006	0.0002	0.0053	0.1446	442594.79	3711.52	181.79	1.51	0.9581	1.4520
quaternary (convex)	0.00002	0.0002	0.0041	0.0759	548562.25	2011.78	173.88	3.37	0.9088	1.6123

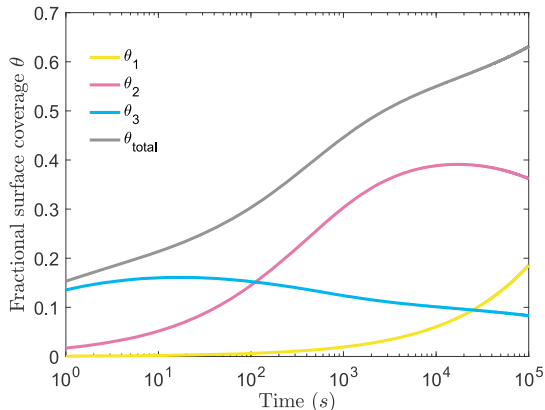


**Figure 6.** Evolution of the fractional surface coverage for each individual component in the ternary mixture model from fitting with Freer and Radke's data. Pseudocomponent 1 (in yellow) is the most surface-active but the lowest fraction; pseudocomponent 3 (in blue) is the most abundant but the least surface-active fraction; the total fractional coverage of the mixture (in gray) increases with time.

Another observation from the optimized results for Freer and Radke's data is that the sum of all of the pseudocomponents' concentrations is approximately in the same order of the nominal concentration, which was calculated using the initial bulk concentration and asphaltenes molecules' average molecular weight of 750 g/mol from the literature.<sup>69,70</sup> For Yarranton's data, the large deviation between the optimized sum and the nominal concentration suggests that their asphaltenes might have a much larger average molecular weight. Moreover, both the majority and the minority fractions exhibit much higher adsorption coefficients compared to the other case.

**3.2. Discussion on the Dominating Fraction in the Asphaltene Mixture.** In previous studies, asphaltene fractions that have the surface-active molecules were found to be responsible to stabilize the water-in-oil emulsion and more difficult to be removed from the interface.<sup>41</sup> The consequence of removing the most surface-active fraction is that the surface coverage will decrease after a certain time as indicated in Figure 6 and the water-in-oil emulsion will become unstable as observed in the recent studies.<sup>41,42</sup>

The wide distribution in the interfacial surface activity of different asphaltene fractions has actually been observed and confirmed by different experimental techniques.<sup>30,41,42</sup> However, the correlation between the surface property or adsorption behavior to the structure of asphaltene molecules, especially the functional groups or molecules, still remains a debate. To identify the dominant factor in asphaltene adsorption behavior, different approaches have been attempted. It is believed that the variations in the adsorption

behaviors or the surface activity among different asphaltene groups are ascribed to the large diversity in the polarity. This was supported by a recent fractionation experiment which found that the most surface-active asphaltene group mainly stayed in the least soluble fraction, i.e., the portion with the highest polarity.<sup>42</sup> It was observed that there was no significant difference in the molecular weights between more polar and less polar fractions. The structure among different fractions was found to be of no significant difference confirmed by FTIR spectroscopy, gel permeation chromatography, and elemental analysis.<sup>39,71</sup> Previous studies on fractionated asphaltenes using inductively coupled plasma spectrometry and X-ray fluorescence analysis indicated that the higher polarity was probably due to the presence of metals and heteroatoms in the polycyclic aromatic hydrocarbons.<sup>39,71</sup> The most polar fraction seems to be the most prone to aggregate in the solution and the aggregation rate was found to be directly proportional to the number of heteroatoms under the electrical field.<sup>72</sup> However, in this experimental evidence, asphaltenes that have been studied are mostly obtained by fractionation based on solubility and the composition and structure of these fractions might not be the same as those of the interfacially active fractions. In a series of articles,<sup>73,74</sup> Xu's group separated the interfacially surface-active asphaltenes from the remaining bulk asphaltenes and performed comprehensive characterization using FTIR, MS, and NMR analyses. It was shown that the interfacially active asphaltenes are different from the bulk remaining asphaltenes in the average molecular representation; i.e., the interfacially active asphaltenes are generally composed of larger molecules with a higher number of heteroatoms. The interfacial asphaltenes are, however, not a single class of compound, and they are just enriched in certain types of molecules compared to the bulk ones. For example, the interfacial material was found to have more oxygen and sulfur than the supernatant, particularly under the form of sulfoxides but not exclusively.<sup>73</sup> It was also observed in the MS results of the whole asphaltenes and the interfacial materials separated at different concentrations<sup>75</sup> that some components are enriched in the interfacial materials and some others are not. This means that some molecules have higher adsorption coefficients than the others and the interfacial material is essentially composed of a mixture of molecules differing in adsorption coefficient. Nonetheless, these molecules should have similar values of  $kC$  (the product of adsorption coefficient and subsurface concentration); otherwise, one would be extremely dominant and the asphaltene class would behave like a single-component system. As various experiments have confirmed, asphaltenes have wide distributions in interfacial activities and composition in different fractions. Nevertheless, no fraction can be claimed to be dominating the interfacial behavior of the whole asphaltenes.

### 3.3. Discussion on the Irreversibility of Asphaltene Adsorption.

One of the qualitative arguments used to support the idea of irreversible asphaltenes adsorption is the wrinkling of water droplets contracted after aging in an asphaltenes solution:<sup>76</sup> as in the case of irreversibly adsorbed particles, a reduction in interfacial area would cause an increase in fractional coverage up to the saturation of the interface and its collapse. The irreversible adsorption is, however, not necessary to observe the collapse, as noted in the first investigations of the relationship between wrinkling and water/crude oil emulsion stability.<sup>77–79</sup> The slow disappearance of wrinkles after droplet contraction (as observed not only for crude-oil/water interfaces but also for asphaltenes-solution/water interfaces<sup>26,80,81</sup>) could be the evidence of a slow desorption.

On a quantitative basis, reversibility of asphaltenes' adsorption was reported in coarsening emulsions: upon a decrease in interfacial area the total mass of asphaltenes adsorbed at the water–oil interface was observed to decrease by up to 40% over the course of 24 h.<sup>76</sup> On the other hand, washout experiments have largely shown that upon replacement of asphaltenes solutions by pure solvent, interfacial tension only partly and slowly recovers (i.e., it does not reincrease up to the clean interface value over an extended period of time).<sup>80,82</sup> However, to conclude from those washout experiments that adsorption is irreversible, one should make sure the duration of washout is long enough for the particular chemical species under investigation.<sup>83</sup>

When washout is performed by replacing the external phase in a pendant droplet experiment in a recent study,<sup>80</sup> a significant hydrodynamic boundary layer can form around the droplet, in which surfactant mass transfer is governed by diffusion. In such a case, desorption kinetics are expected to be commensurate with adsorption kinetics and washout should at least be of the same duration as the initial adsorption. A safety margin should even be applied in case adsorption has not reached equilibrium before washout, because surfactant concentration could still be lower in the immediate vicinity of the interface than further away in solution (otherwise mixing associated with washout would first cause an increase in surfactant concentration close to the interface). Those conditions are probably not satisfied in this study.

When washout is performed by replacing the internal phase,<sup>81</sup> the hydrodynamic boundary layer is extremely thin and desorption kinetics are to be controlled by the energy barrier to desorption. In the simplest case, this energy barrier is directly related to the adsorption constant of the surfactant: the more surface-active the surfactant, the slower the desorption. The situation gets more complex when the surfactant solution contains a variety of molecules with diverse surface activity, as is the case for asphaltenes:<sup>30,41,84</sup> each surfactant will desorb according to its own surface activity. When the replacement of the surrounding solution by pure solvent starts in the washout experiment, due to the mixing of the fluids, the local concentration of asphaltenes' most surface-active components close to the boundary layer exhibits an instantaneous increase in the initial few seconds. The equilibrium of these fractions at the interface has not been established yet before the desorption experiment starts. The concentration gradient between the bulk solution and the subsurface layer for these fractions still exists and provides the driving force for their diffusion and adsorption (see Figure 7). This means that, for a while, the washout will not cause any desorption because the concentration away from the interface

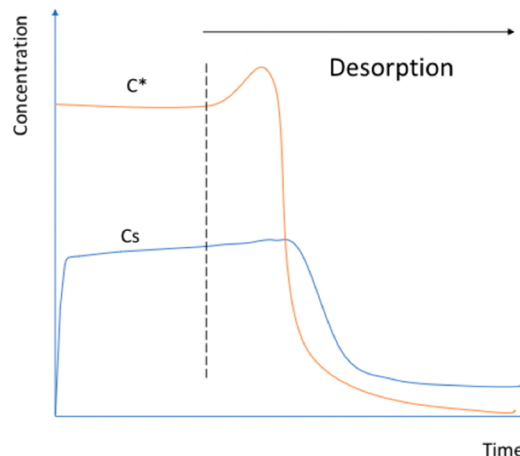


**Figure 7.** Illustration of the concentration evolution during washout ( $C^*$  is the concentration close to the boundary layer, and  $C_s$  is the concentration in the subsurface layer).

will be higher than that close to the interface. Unlike the majority asphaltenes molecules, the most surface-active group keeps moving toward the subsurface layer for a while. The interfacial tension maintains almost the same since the desorption of the abundant and less surface-active group from the interface frees up more adsorption sites available for the more surface-active molecules to adsorb. After the initial few seconds, the concentration of the most surface-active fractions close to the boundary layer reaches the maximum and then starts to decrease under the mixed kinetics of diffusion and convection. The subsurface concentration of these fractions keeps increasing until it becomes larger than the concentration near the boundary layer. The desorption of the most surface-active fractions starts only when the concentration profile exhibits a monotonic slope. The kinetics is initially accelerated and then controlled by a mixed mechanism of diffusion and convection.

The presence of the minority components of high activity but low concentration (as inferred from the analysis of dilatational rheology data by a diffusion-controlled adsorption model<sup>29</sup>) would then explain the slow and “stepwise” desorption reported in the earlier studies.<sup>85</sup> Such a scenario would also explain why wrinkling appears to be less and less reversible as time passes by as reported: the longer the adsorption time, the higher the proportion of asphaltenes with high adsorption coefficient at the interface and hence the slower desorption. It would finally enable resolving the apparent contradiction between the observation of “irreversibility” of asphaltenes’ adsorption at the scale of a single droplet and reversibility of adsorption at the scale of an emulsion. For a pendant drop, the ratio of droplet volume (asphaltenes’ reservoir) to interfacial area (asphaltenes’ sink) is approximately equal to  $R$ , the diameter of the droplet, which is typically 2 mm. For the water-in-oil emulsion, the ratio of supernatant volume to droplet area is equal to  $d_{32}/2 \times (1 - v_{\text{water}})/v_{\text{water}}$  with  $d_{32}$  the Sauter mean diameter and  $v_f$  the volume fraction of water. With a 40% water volume fraction and a mean Sauter diameter ca. 10  $\mu\text{m}$  (data from Yarranton et al.<sup>76</sup>), the volume/area ratio becomes equal to 15  $\mu\text{m}$ . Depletion effects imply that the fractional area covered by minority components of high activity will be much larger in the

emulsion than in the pendant droplet setup, which would make desorption more pronounced in the emulsion.

**3.4. Dilatation Rheology after Long-Time Asphaltenes Adsorption.** With the same underlying physics, i.e., the diffusion-controlled process, the optimized parameters extracted from the quantitative fit between the multicomponent mixture model and experimental dynamic interfacial tension data could further be used to predict the rheology for the same asphaltene solution. Using the optimized initial bulk concentrations, the subsurface concentrations after long-time adsorption can be numerically computed from the Ward–Tordai equation. The corresponding dilatational moduli were then computed using the previously reported inversion matrix method,<sup>44</sup> and the predicted numerical values were plotted against the corresponding experimental data in Figure 8 and Figure 9.

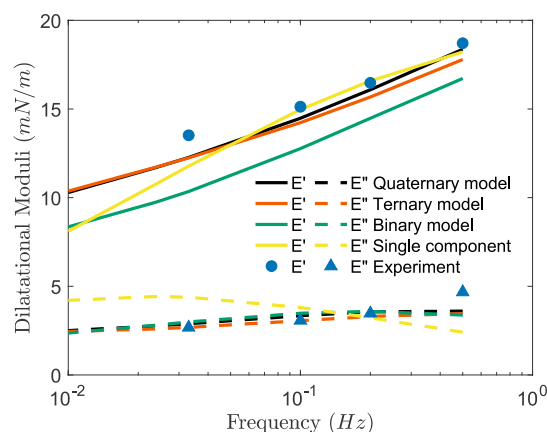


**Figure 8.** Numerical dilatational rheology curve generated using the optimized result from multicomponent mixture model. Experimental data from Sztukowski and Yarranton:<sup>11</sup> 0.5 kg/m<sup>3</sup> asphaltenes in toluene, aging time 16 h.

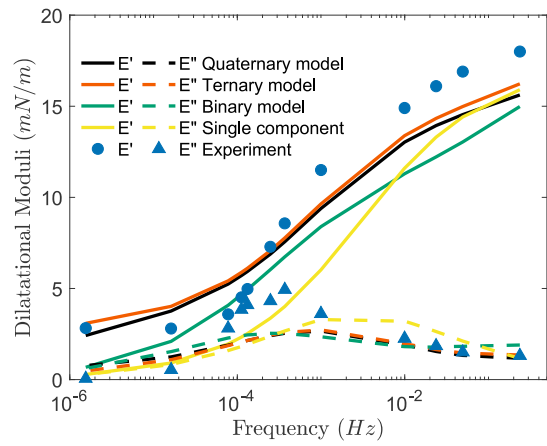


**Figure 9.** Numerical dilatational rheology curve generated using the optimized result from multicomponent mixture model. Experimental data from Freer and Radke:<sup>16</sup> 0.005 wt % asphaltenes in toluene, aging time 24 h.

Compared to the single-component and binary system, the predicted elastic and viscous moduli values by ternary and quaternary systems show smaller deviations from the experiment data. Similar to the observations in interfacial tensions,

adding a fourth pseudocomponent to the mixture model did not produce a significant improvement on the predictions.

In Yarranton's case, the experiment only tested four points in the two frequency decades, which is not adequate to show the full picture of moduli variations with frequencies. However, the current mixture model enables the predictions of dilatational rheology data for the missing frequency decades and provides insight into how the asphaltenes-covered interface behaves when experimental data are expensive to obtain. The performance of the developed model was further assessed in Freer and Radke's case, where the predicted moduli match fairly well with experimental data. The deviation of the generated moduli curve from the experimental one in the low frequency range might be contributed to by the effect of reduced curvature, which is not incorporated in the current model and will be discussed later. This effect could be less dominant when the frequency increases. One can also observe that the generated elastic moduli curve deviated from the experimental data at high frequencies. That is because the selected equilibrium equation of state tends to underestimate the limiting elasticity, the high-frequency elasticity, for the same surface pressure.

After a long period of adsorption, the subsurface near the asphaltenes-laden interface is predominantly occupied by the most surface-active components as observed in the previous fractional surface coverage curve. Hence, the evolution of viscoelastic behaviors of the asphaltenes-laden interface with aging time is primarily led by the prolonged equilibration of the most surface-active fractions.

**3.5. Simultaneous Optimization of Multiple Dynamic Interfacial Tension Curves' Adsorption Isotherm.** With the computational methods that we have developed for the current diffusion-controlled mixture model, it enables one to analyze multiple data sets simultaneously with the same set of adsorption parameters but different composition within a reasonable simulation time. In order to examine how different fractions vary with the total bulk concentration, experimental data from Sztukowski and Yarranton<sup>11</sup> for three different concentrations were analyzed using the ternary mixture model (see Figure 10), and the optimized variables are summarized in Table 6.

As the total concentration increases, the optimized concentration of the most surface-active fraction almost has no variation and the fraction with intermediate adsorption parameters shows a little increase in concentration. The majority fraction, which is the least surface-active, exhibits a proportional increase with the mixture concentration. These trends could be clearly observed when plotting the optimized concentration from each IFT data set versus the respective nominal concentration (see Figure 11).

The evolution in the concentrations of the three pseudocomponents can well explain what was observed in the previous work where nanoaggregation of asphaltenes in toluene was studied using NMR spectroscopy.<sup>27</sup> The bimodal increase in the NMR signal of asphaltenes' samples<sup>27,65,67</sup> and conductivity measurement<sup>68</sup> can be justified by the finding that the most surface-active component levels off after a critical concentration and the majority fraction keeps increasing with the total concentrations. This also supported the consensus that the most surface-active component in an asphaltenes' group is the fraction that is most prone to nanoaggregate.<sup>86</sup>

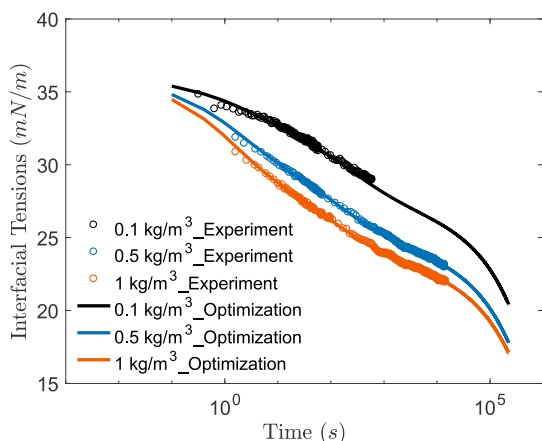


**Figure 10.** Comparison of numerical data generated from simultaneous optimizations of experimental data at three different concentrations using a ternary mixture model. Experimental data from Sztukowski and Yarranton<sup>11</sup> (by empty circles): asphaltenes in toluene with the concentration of 0.1 kg/m<sup>3</sup> (in black), 0.5 kg/m<sup>3</sup> (in blue), and 1 kg/m<sup>3</sup> (in vermillion).

**Table 6. Optimized Variables from Simultaneous Optimization of Multiple IFT Curves Using Ternary Mixture Model**

	$C_{b1}$ (mol/m <sup>3</sup> )	$C_{b2}$ (mol/m <sup>3</sup> )	$C_{b3}$ (mol/m <sup>3</sup> )
$C_0 = 0.1 \text{ kg/m}^3$	0.00006	0.00788	0.05115
$C_0 = 0.5 \text{ kg/m}^3$	0.00029	0.01009	0.10834
$C_0 = 1.0 \text{ kg/m}^3$	0.00026	0.01153	0.13025
	$k_1$ (m <sup>3</sup> /mol)	$k_2$ (m <sup>3</sup> /mol)	$k_3$ (m <sup>3</sup> /mol)
for multicurves	4334524	88.59	4.63

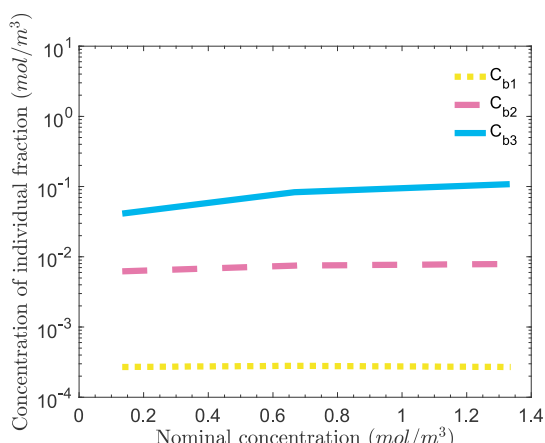


**Figure 11.** Optimized individual concentrations versus nominal concentrations.

## 4. CONCLUSION

The dynamic interfacial tensions from asphaltenes' adsorption kinetics were studied using a diffusion-controlled ternary and quaternary mixture model. The numerical and optimization methods to solve the nonlinear governing equations for a multicomponent system have been demonstrated and validated against both experimental data and numerical solutions from Van den Bogaert and Joos.<sup>52</sup> From the analysis of experimental IFT data from Sztukowski and Yarranton<sup>11</sup> and Freer and Radke<sup>16</sup> using the developed computational methods, a ternary mixture model proved to capture the evolution of IFTs from a

few seconds up to 24 h very well and enable a fairly precise prediction of dilatational rheology over 7 frequency decades. From the optimization with the multicomponent mixture model, it was found that the most surface-active asphaltenes fraction is less than 1% and the optimized initial concentrations of all pseudocomponents approximately add up to the nominal bulk concentrations. Compared to the single-component and binary mixture model, the introduction of the additional pseudocomponent makes the mixture model able to preserve the fast equilibration of the majority fractions at short times while well predicting the long-term dilatational rheology. The minority surface-active molecules, which are enriched in the interfacially active asphaltenes as observed in previous studies,<sup>41,73</sup> are probably the asphaltene molecules with larger sizes and more heteroatoms in their structure. The consequences for the presence of such different adsorption parameters in various fractions of asphaltene solubility class are that the bulk IFTs can keep decreasing for a long time as predicted by the mixture model and no sign of equilibration was observed within the simulation time. This hypothesis was confirmed by the recent fractionation experiment where the water-in-oil emulsion proved to be unstable with the interfacially active fraction removed.<sup>42</sup> From the simultaneous optimization of the IFT data sets at three different concentrations, the most surface-active component was found to stop increasing after a critical concentration while the majority fraction keeps increasing with the total concentrations.

The ternary mixture model enables the explanation of the discrepancy between the long-time equilibration observed during the experiment and the characteristic time scale of a diffusion-controlled adsorption process while retaining the characteristics of fast decrease in surface tensions by a typical representation of the polydispersity of the whole asphaltene mixture. Although ternary mixture model gives better fitting, as the number of the to-be-optimized variables increases, the complexity of the optimization problem and the computational time also confronts an exponential increase. Nevertheless, this can be compensated for by implementing a larger time discretization and allowing a larger tolerance for selected numerical methods.

## ASSOCIATED CONTENT

### Supporting Information

The Supporting Information is available free of charge at <https://pubs.acs.org/doi/10.1021/acs.energyfuels.0c02421>.

Sensitivity analysis on the surface excess coverage and diffusion coefficient and comparison of predicted and experimental interfacial tensions (PDF)

## AUTHOR INFORMATION

### Corresponding Author

Fang Liu – Tandon School of Engineering, New York University, Brooklyn, New York 11201, United States; [orcid.org/0000-0001-7382-6215](https://orcid.org/0000-0001-7382-6215); Email: [fangliu@nyu.edu](mailto:fangliu@nyu.edu)

### Authors

Vincent Pauchard – Department of Chemical Engineering, City College of New York, New York, New York 10031, United States; [orcid.org/0000-0003-1027-4526](https://orcid.org/0000-0003-1027-4526)

Sanjoy Banerjee — Energy Institute and Department of Chemical Engineering, City College of New York, New York, New York 10031, United States

Complete contact information is available at:  
<https://pubs.acs.org/10.1021/acs.energyfuels.0c02421>

## Notes

The authors declare no competing financial interest.

§ Consultant for SINTEF Industry, Norway.

## ACKNOWLEDGMENTS

We thank Prof. Charles Maldarelli, Prof. Lamia Goual, Dr. Oliver Mullins, and Mr. Bo Lin for inspiring discussions and Prof. Harvey Yarranton for generously sharing his unpublished experimental data. We are also grateful to the technical support from the Benjamin Levich Institute computing services and CUNY high performance computing center (HPCC). The CUNY HPCC is operated by the College of Staten Island and funded, in part, by grants from the City of New York, State of New York, CUNY Research Foundation, and National Science Foundation Grants CNS-0958379, CNS-0855217, and ACI 1126113. This material is based upon work supported by the National Science Foundation under Award No. 1743794.

## REFERENCES

- (1) Rane, J. P.; et al. Applicability of the Langmuir Equation of State for Asphaltene Adsorption at the Oil–Water Interface: Coal-Derived, Petroleum, and Synthetic Asphaltenes. *Energy Fuels* **2015**, *29*, 3584–3590.
- (2) Rane, J. P.; Harbottle, D.; Pauchard, V.; Couzis, A.; Banerjee, S. Adsorption Kinetics of Asphaltenes at the Oil–Water Interface and Nanoaggregation in the Bulk. *Langmuir* **2012**, *28*, 9986–9995.
- (3) Fan, Y.; Simon, S.; Sjöblom, J. Interfacial shear rheology of asphaltenes at oil–water interface and its relation to emulsion stability: Influence of concentration, solvent aromaticity and nonionic surfactant. *Colloids Surf, A* **2010**, *366*, 120–128.
- (4) Schuler, B. et al. Overview of Asphaltene Nanostructures and Thermodynamic Applications. *Energy Fuels* **0**, [acs.energyfuels.0c00874](https://pubs.acs.org/10.1021/acs.energyfuels.0c00874)
- (5) Liu, F. Understanding Asphaltenes Adsorption at Liquid–Liquid and Liquid–Solid Interfaces. Ph.D. Thesis, City College of New York, New York, 2020.
- (6) Rane, J. P.; Pauchard, V.; Couzis, A.; Banerjee, S. Interfacial rheology of asphaltenes at oil–water interfaces and interpretation of the equation of state. *Langmuir* **2013**, *29*, 4750–4759.
- (7) Pauchard, V.; Rane, J. P.; Zarkar, S.; Couzis, A.; Banerjee, S. Long-Term Adsorption Kinetics of Asphaltenes at the Oil–Water Interface: A Random Sequential Adsorption Perspective. *Langmuir* **2014**, *30*, 8381–8390.
- (8) Samaniuk, J. R.; Hermans, E.; Verwijlen, T.; Pauchard, V.; Vermant, J. Soft-Glassy Rheology of Asphaltenes at Liquid Interfaces. *J. Dispersion Sci. Technol.* **2015**, *36*, 1444–1451.
- (9) Goual, L.; Horváth-Szabó, G.; Masliyah, J. H.; Xu, Z. Adsorption of Bituminous Components at Oil/Water Interfaces Investigated by Quartz Crystal Microbalance: Implications to the Stability of Water-in-Oil Emulsions. *Langmuir* **2005**, *21*, 8278–8289.
- (10) Lin, Y.-J.; et al. Combined interfacial shear rheology and microstructure visualization of asphaltenes at air–water and oil–water interfaces. *J. Rheol. (Melville, NY, U. S.)* **2018**, *62*, 1–10.
- (11) Sztukowski, D. M.; Yarranton, H. W. Rheology of Asphaltene–Toluene/Water Interfaces. *Langmuir* **2005**, *21*, 11651–11658.
- (12) Specker, P. M.; Kilpatrick, P. K. Interfacial Rheology of Petroleum Asphaltenes at the Oil–Water Interface. *Langmuir* **2004**, *20*, 4022–4032.
- (13) Aske, N.; Orr, R.; Sjöblom, J. Dilatational Elasticity Moduli of Water–Crude Oil Interfaces Using the Oscillating Pendant Drop. *J. Dispersion Sci. Technol.* **2002**, *23*, 809–825.
- (14) Jeribi, M.; Almir-Assad, B.; Langevin, D.; Hénaut, I.; Argillier, J. F. Adsorption Kinetics of Asphaltenes at Liquid Interfaces. *J. Colloid Interface Sci.* **2002**, *256*, 268–272.
- (15) Sheu, E.; Storm, D. A.; Shields, M. B. Adsorption kinetics of asphaltenes at toluene/acid solution interface. *Fuel* **1995**, *74*, 1475–1479.
- (16) Freer, E. M.; Radke, C. J. Relaxation of Asphaltenes At the Toluene/Water Interface: Diffusion Exchange and Surface Rearrangement. *J. Adhes.* **2004**, *80*, 481–496.
- (17) Bouriat, P.; El Kerri, N.; Graciaa, A.; Lachaise, J. Properties of a Two-Dimensional Asphaltene Network at the Water–Cyclohexane Interface Deduced from Dynamic Tensiometry. *Langmuir* **2004**, *20*, 7459–7464.
- (18) Pauchard, V.; et al. Role of Naphthenic Acids in Emulsion Tightness for a Low-Total-Acid-Number (TAN)/High-Asphaltenes Oil. *Energy Fuels* **2009**, *23*, 1269–1279.
- (19) Dicharry, C.; Arla, D.; Sinquin, A.; Graciaa, A.; Bouriat, P. Stability of water/crude oil emulsions based on interfacial dilatational rheology. *J. Colloid Interface Sci.* **2006**, *297*, 785–791.
- (20) Anton, N.; Vandamme, T. F.; Bouriat, P. Dilatational rheology of a gel point network formed by nonionic soluble surfactants at the oil–water interface. *Soft Matter* **2013**, *9*, 1310–1318.
- (21) Aske, N.; Kallevik, H.; Sjöblom, J. Water-in-crude oil emulsion stability studied by critical electric field measurements. Correlation to physico-chemical parameters and near-infrared spectroscopy. *J. Pet. Sci. Eng.* **2002**, *36*, 1–17.
- (22) McLean, J.; Kilpatrick, P. Effects of Asphaltene Aggregation in Model Heptane–Toluene Mixtures on Stability of Water-in-Oil Emulsions. *J. Colloid Interface Sci.* **1997**, *196*, 23–34.
- (23) Angle, C. W.; Hua, Y. Dilational Interfacial Rheology for Increasingly Deasphalted Bitumens and n-C<sub>5</sub> Asphaltenes in Toluene/NaHCO<sub>3</sub> Solution. *Energy Fuels* **2012**, *26*, 6228–6239.
- (24) Hannisdal, A.; Orr, R.; Sjöblom, J. Viscoelastic Properties of Crude Oil Components at Oil–Water Interfaces. 1. The Effect of Dilution. *J. Dispersion Sci. Technol.* **2007**, *28*, 81–93.
- (25) Pauchard, V.; Roy, T. Blockage of coalescence of water droplets in asphaltenes solutions: A jamming perspective. *Colloids Surf, A* **2014**, *443*, 410–417.
- (26) Pauchard, V.; Rane, J. P.; Banerjee, S. Asphaltene–Laden Interfaces Form Soft Glassy Layers in Contraction Experiments: A Mechanism for Coalescence Blocking. *Langmuir* **2014**, *30*, 12795–12803.
- (27) Zarkar, S.; Pauchard, V.; Farooq, U.; Couzis, A.; Banerjee, S. Interfacial Properties of Asphaltenes at Toluene–Water Interfaces. *Langmuir* **2015**, *31*, 4878–4886.
- (28) Sztukowski, D. M.; Jafari, M.; Alboudwarej, H.; Yarranton, H. W. Asphaltene self-association and water-in-hydrocarbon emulsions. *J. Colloid Interface Sci.* **2003**, *265*, 179–186.
- (29) Liu, F.; et al. Mixture Effect on the Dilatation Rheology of Asphaltenes–Laden Interfaces. *Langmuir* **2017**, *33*, 1927–1942.
- (30) Fossen, M.; Kallevik, H.; Knudsen, K. D.; Sjöblom, J. Asphaltenes Precipitated by a Two-Step Precipitation Procedure. 2. Physical and Chemical Characteristics. *Energy Fuels* **2011**, *25*, 3552–3567.
- (31) Schuler, B.; Meyer, G.; Peña, D.; Mullins, O. C.; Gross, L. Unraveling the Molecular Structures of Asphaltenes by Atomic Force Microscopy. *J. Am. Chem. Soc.* **2015**, *137*, 9870–9876.
- (32) Speight, J. G. Petroleum Asphaltenes - Part 1: Asphaltenes, Resins and the Structure of Petroleum. *Oil Gas Sci. Technol.* **2004**, *59*, 467–477.
- (33) Tavakkoli, M.; Panuganti, S. R.; Taghikhani, V.; Pishvaie, M. R.; Chapman, W. G. Understanding the polydisperse behavior of asphaltenes during precipitation. *Fuel* **2014**, *117*, 206–217.
- (34) Mullins, O. C. The Modified Yen Model. *Energy Fuels* **2010**, *24*, 2179–2207.

(35) Mullins, O. C.; et al. Advances in Asphaltene Science and the Yen-Mullins Model. *Energy Fuels* **2012**, *26*, 3986–4003.

(36) Gutiérrez, L. B.; Ranaudo, M. A.; Méndez, B.; Acevedo, S. Fractionation of Asphaltene by Complex Formation with p-Nitrophenol. A Method for Structural Studies and Stability of Asphaltene Colloids. *Energy Fuels* **2001**, *15*, 624–628.

(37) Qiao, P.; et al. Fractionation of Asphaltenes in Understanding Their Role in Petroleum Emulsion Stability and Fouling. *Energy Fuels* **2017**, *31*, 3330–3337.

(38) Fossen, M.; Sjøblom, J.; Kallevik, H.; Jakobsson, J. A New Procedure for Direct Precipitation and Fractionation of Asphaltenes from Crude Oil. *J. Dispersion Sci. Technol.* **2007**, *28*, 193–197.

(39) Kaminski, T. J.; Fogler, H. S.; Wolf, N.; Wattana, P.; Mairal, A. Classification of Asphaltenes via Fractionation and the Effect of Heteroatom Content on Dissolution Kinetics. *Energy Fuels* **2000**, *14*, 25–30.

(40) Acevedo, S.; et al. Observations about the Structure and Dispersion of Petroleum Asphaltenes Aggregates Obtained from Dialysis Fractionation and Characterization †. *Energy Fuels* **1997**, *11*, 774–778.

(41) Yang, F.; et al. Asphaltene Subfractions Responsible for Stabilizing Water-in-Crude Oil Emulsions. Part 1: Interfacial Behaviors. *Energy Fuels* **2014**, *28*, 6897–6904.

(42) Rocha, J. A.; Baydak, E. N.; Yarranton, H. W. What Fraction of the Asphaltenes Stabilizes Water-in-Bitumen Emulsions? *Energy Fuels* **2018**, *32*, 1440–1450.

(43) Xu, Y.; Dabros, T.; Hamza, H.; Shefantook, W. Destabilization of water in bitumen emulsion by washing with water. *Pet. Sci. Technol.* **1999**, *17*, 1051–1070.

(44) Liu, F.; Akhmetkhanova, N.; Pauchard, V. A simple numerical solution of diffusional equations for dilatational rheology of complex surfactant mixtures in any geometry. *Colloids Surf, A* **2017**, *532*, 140–143.

(45) Danov, K. D.; Kralchevsky, P. A.; Denkov, N. D.; Ananthapadmanabhan, K. P.; Lips, A. Mass transport in micellar surfactant solutions: 2. Theoretical modeling of adsorption at a quiescent interface. *Adv. Colloid Interface Sci.* **2006**, *119*, 17–33.

(46) Ward, A. F. H.; Tordai, L. Time-Dependence of Boundary Tensions of Solutions I. The Role of Diffusion in Time-Effects. *J. Chem. Phys.* **1946**, *14*, 453.

(47) Daniel, R. C.; Berg, J. C. Dynamic surface tension of polydisperse surfactant solutions: A pseudo-single-component approach. *Langmuir* **2002**, *18*, 5074–5082.

(48) Ravera, F.; Liggieri, L.; Steinchen, A. Sorption kinetics considered as a renormalized diffusion process. *J. Colloid Interface Sci.* **1993**, *156*, 109–116.

(49) Miller, R.; Kretzschmar, G. Adsorption kinetics of surfactants at fluid interfaces. *Adv. Colloid Interface Sci.* **1991**, *37*, 97–121.

(50) Lin, S.-Y.; McKeigue, K.; Maldarelli, C. Diffusion-Controlled Surfactant Adsorption Studied by Pendant Drop Digitization. *AIChE J.* **1990**, *36*, 1785–1795.

(51) Arias, S. I.; et al. An axisymmetric model for the analysis of dynamic surface tension. *RSC Adv.* **2015**, *5*, 7921–7931.

(52) Van den Bogaert, R.; Joos, P. Diffusion-controlled adsorption kinetics for a mixture of surface active agents at the solution-air interface. *J. Phys. Chem.* **1980**, *84*, 190–194.

(53) Lucassen, J.; Van Den Tempel, M. Dynamic measurements of dilatational properties of a liquid interface. *Chem. Eng. Sci.* **1972**, *27*, 1283–1291.

(54) Aksenenko, E. V.; Kovalchuk, V. I.; Fainerman, V. B.; Miller, R. Surface dilatational rheology of mixed adsorption layers at liquid interfaces. *Adv. Colloid Interface Sci.* **2006**, *122*, 57–66.

(55) Goodfellow, I.; Bengio, Y.; Courville, A. *Deep Learning*. (MIT Press, 2016).

(56) Broyden, C. G. The Convergence of a Class of Double-rank Minimization Algorithms 1. General Considerations. *IMA J. Appl. Math.* **1970**, *6*, 76–90.

(57) Goldfarb, D. A family of variable-metric methods derived by variational means. *Math. Comput.* **1970**, *24*, 23–23.

(58) Fletcher, R. A new approach to variable metric algorithms. *Comput. J.* **1970**, *13*, 317–322.

(59) Shanno, D. F.; Kettler, P. C. Optimal conditioning of quasi-Newton methods. *Math. Comput.* **1970**, *24*, 657–657.

(60) Shanno, D. F. Conditioning of quasi-Newton methods for function minimization. *Math. Comput.* **1970**, *24*, 647–647.

(61) Sztukowski, D. M.; Yarranton, H. M. Characterization and interfacial behavior of oil sands solids implicated in emulsion stability. *J. Dispersion Sci. Technol.* **2004**, *25*, 299–310.

(62) Gafanova, O. V.; Yarranton, H. W. The Stabilization of Water-in-Hydrocarbon Emulsions by Asphaltenes and Resins. *J. Colloid Interface Sci.* **2001**, *241*, 469–478.

(63) Freer, E. M.; Svitova, T.; Radke, C. J. The Role of Interfacial Rheology in Reservoir Mixed Wettability. *J. Pet. Sci. Eng.* **2003**, *39*, 137–158.

(64) Liu, F.; Hickman, S.; Maqbool, T.; Pauchard, V.; Banerjee, S. Study of Asphaltene Deposition onto Stainless-Steel Surfaces Using Quartz Crystal Microbalance with Dissipation. *Energy Fuels* **2020**, *34*, 9283–9295.

(65) Durand, E.; et al. 1 H Diffusion-Ordered Spectroscopy (DOSY) Nuclear Magnetic Resonance (NMR) as a Powerful Tool for the Analysis of Hydrocarbon Mixtures and Asphaltenes. *Energy Fuels* **2008**, *22*, 2604–2610.

(66) Norinaga, K.; Wargardalam, V. J.; Takasugi, S.; Iino, M.; Matsukawa, S. Measurement of Self-Diffusion Coefficient of Asphaltene in Pyridine by Pulsed Field Gradient Spin-Echo 1 H NMR. *Energy Fuels* **2001**, *15*, 1317–1318.

(67) Lisitza, N. V.; Freed, D. E.; Sen, P. N.; Song, Y.-Q. Study of Asphaltene Nanoaggregation by Nuclear Magnetic Resonance (NMR) †. *Energy Fuels* **2009**, *23*, 1189–1193.

(68) Goual, L.; Abudu, A. Predicting the Adsorption of Asphaltenes from Their Electrical Conductivity. *Energy Fuels* **2010**, *24*, 469–474.

(69) Groenin, H.; Mullins, O. C. Asphaltene Molecular Size and Structure. *J. Phys. Chem. A* **1999**, *103*, 11237–11245.

(70) Qian, K.; Rodgers, R. P.; Hendrickson, C. L.; Emmett, M. R.; Marshall, A. G. Reading Chemical Fine Print: Resolution and Identification of 3000 Nitrogen-Containing Aromatic Compounds from a Single Electrospray Ionization Fourier Transform Ion Cyclotron Resonance Mass Spectrum of Heavy Petroleum Crude Oil. *Energy Fuels* **2001**, *15*, 492–498.

(71) Nalwaya, V.; Tantayakom, V.; Piumsomboon, P.; Fogler, S. Studies on asphaltenes through analysis of polar fractions. *Ind. Eng. Chem. Res.* **1999**, *38*, 964–972.

(72) Hosseini, A.; et al. Electrokinetic behavior of asphaltene particles. *Fuel* **2016**, *178*, 234–242.

(73) Yang, F.; et al. Asphaltene Subfractions Responsible for Stabilizing Water-in-Crude Oil Emulsions. Part 2: Molecular Representations and Molecular Dynamics Simulations. *Energy Fuels* **2015**, *29*, 4783–4794.

(74) Qiao, P.; Harbottle, D.; Tchoukov, P.; Wang, X.; Xu, Z. Asphaltene Subfractions Responsible for Stabilizing Water-in-Crude Oil Emulsions. Part 3. Effect of Solvent Aromaticity. *Energy Fuels* **2017**, *31*, 9179–9187.

(75) Czarnecki, J. Stabilization of Water in Crude Oil Emulsions. Part 2 †. *Energy Fuels* **2009**, *23*, 1253–1257.

(76) Yarranton, H. W.; Urrutia, P.; Sztukowski, D. M. Effect of interfacial rheology on model emulsion coalescence. II. Emulsion coalescence. *J. Colloid Interface Sci.* **2007**, *310*, 253–259.

(77) Harvey, R. R. Theoretical approach to the investigation of films occurring at crude oil-water interfaces. *Trans. Soc. Pet. Eng.* **1960**, *219*, 350–353.

(78) Bartell, F. E.; Benner, F. C. Adsorption at solid-liquid interfaces Determination of adsorption by adhesion-tension and interfacial-tension measurements on binary organic liquid systems. *J. Phys. Chem.* **1942**, *46*, 847–859.

(79) Strassner, J. E. Effect of pH on Interfacial Films and Stability of Crude Oil-Water Emulsions. *JPT, J. Pet. Technol.* **1968**, *20*, 303–312.

(80) Freer, E. M.; Radke, C. J. Relaxation of asphaltenes at the toluene/water interface: diffusion exchange and surface rearrangement. *J. Adhes.* **2004**, *80*, 481–496.

(81) Yarranton, H. W.; Sztukowski, D. M.; Urrutia, P. Effect of interfacial rheology on model emulsion coalescence. I. Interfacial rheology. *J. Colloid Interface Sci.* **2007**, *310*, 246–252.

(82) Pradilla, D.; Simon, S.; Sjöblom, J. Mixed Interfaces of Asphaltenes and Model Demulsifiers, Part II: Study of Desorption Mechanisms at Liquid/Liquid Interfaces. *Energy Fuels* **2015**, *29*, 5507–5518.

(83) Fainerman, V. B.; Leser, M. E.; Michel, M.; Lucassen-Reynders, E. H.; Miller, R. Kinetics of the Desorption of Surfactants and Proteins from Adsorption Layers at the Solution/Air Interface. *J. Phys. Chem. B* **2005**, *109*, 9672–9677.

(84) Acevedo, S.; Borges, B.; Quintero, F.; Piscitelly, V.; Gutierrez, L. B. Asphaltenes and Other Natural Surfactants from Cerro Negro Crude Oil. Stepwise Adsorption at the Water/Toluene Interface: Film Formation and Hydrophobic Effects. *Energy Fuels* **2005**, *19*, 1948–1953.

(85) Pradilla, D.; Simon, S.; Sjöblom, J. Mixed interfaces of asphaltenes and model demulsifiers part I: Adsorption and desorption of single components. *Colloids Surf., A* **2015**, *466*, 45–56.

(86) Spiecker, P. M.; Gawrys, K. L.; Kilpatrick, P. K. Aggregation and solubility behavior of asphaltenes and their subfractions. *J. Colloid Interface Sci.* **2003**, *267*, 178–193.